THE JOURNAL OF BIOLOGICAL CHEMISTRY VOL. 285, NO. 22, pp. 17253–17262, May 28, 2010

Prolyl 3-Hydroxylase 1 Null Mice Display Abnormalities in Fibrillar Collagen-rich Tissues Such as Tendons, Skin, and Bones*[S]

Received for publication, January 7, 2010, and in revised form, March 11, 2010 Published, JBC Papers in Press, April 2, 2010, DOI 10.1074/jbc.M110.102228

Janice A. Vranka[‡], Elena Pokidysheva[‡§], Lauren Hayashi[‡], Keith Zientek[‡], Kazunori Mizuno[‡], Yoshihiro Ishikawa[‡], Kerry Maddox[‡], Sara Tufa[‡], Douglas R. Keene[‡], Robert Klein[¶], and Hans Peter Bächinger[‡§1]

From the [‡]Research Department, Shriners Hospitals for Children, Portland, Oregon 97239, the [§]Department of Biochemistry and Molecular Biology, Oregon Health & Science University, Portland, Oregon 97239, and the [¶]Bone and Mineral Unit, Oregon Health & Science University, Portland, Oregon 97239

Osteogenesis imperfecta (OI) is a skeletal disorder primarily caused by mutations in the type I collagen genes. However, recent investigations have revealed that mutations in the genes encoding for cartilage-associated protein (CRTAP) or prolyl 3-hydroxylase 1 (P3H1) can cause a severe, recessive form of OI. These reports show minimal 3-hydroxylation of key proline residues in type I collagen as a result of CRTAP or P3H1 deficiency and demonstrate the importance of P3H1 and CRTAP to bone structure and development. P3H1 and CRTAP have previously been shown to form a stable complex with cyclophilin B, and P3H1 was shown to catalyze the 3-hydroxylation of specific proline residues in procollagen I *in vitro*. Here we describe a mouse model in which the P3H1 gene has been inactivated. Our data demonstrate abnormalities in collagen fibril ultrastructure in tendons from P3H1 null mice by electron microscopy. Differences are also seen in skin architecture, as well as in developing limbs by histology. Additionally bone mass and strength were significantly lower in the P3H1 mice as compared with wild-type littermates. Altogether these investigations demonstrate disturbances of collagen fiber architecture in tissues rich in fibrillar collagen, including bone, tendon, and skin. This model system presents a good opportunity to study the underlying mechanisms of recessive OI and to better understand its effects in humans.

Osteogenesis imperfecta (OI)[2] is an autosomal dominant genetic disorder and is primarily caused by mutations in the genes encoding for type I collagen (*COL1A1* and *COL1A2*). It is characterized as a heterogeneous group of conditions with varying degrees of severity, including bone fragility, low bone mass, susceptibility to fracture, short stature, bowing of the long bones, and moderate to severe kyphoscoliosis (1–3). Recessive OI cases have been reported more recently and have been shown to be caused by mutations in the cartilage-associated protein (CRTAP), prolyl 3-hydroxylase 1 or leprecan (*LEPRE1*) gene and cyclophilin B (CypB) (4–9). The majority of these more recently described patients have been shown to have severe to lethal forms of autosomal recessive OI with some distinctive features (5–6, 10). The 3-hydroxylation of key residues in collagen I from these patients was significantly reduced indicating the importance of P3H1 and CRTAP in collagen stability, secretion, and ultimately in bone development. Additionally, the importance of CRTAP in bone development was demonstrated in CRTAP knock-out mice, which show osteochondrodysplasia characterized by severe osteoporosis and decreased osteoid production (4). The CypB knock-out mouse also shows severe OI (11). P3H1 has been shown to be responsible for the modification of the proline into 3(*S*)-hydroxyproline in the Xaa position of the Gly-Xaa-Yaa repeating sequence of the alpha 1 chain of type I procollagen (12). It is likely that this enzyme also catalyzes modifications in types II and III collagen as well, although this has not yet been shown (13). P3H1 extracted from chick embryos was also shown to form a stable multiprotein complex with CRTAP and CypB (4, 12). The importance of this protein complex has been demonstrated with the reports of the severely affected phenotypes in the CRTAP and CypB null mice and human mutations in P3H1, CRTAP, and CypB (9). In addition, the P3H1·CRTAP·CypB complex was recently shown to be not only responsible for the 3-hydroxylation of proline residues, but also to act as a potent molecular chaperone (14). Mutations in P3H1, therefore, may affect its various functions during collagen biosynthesis resulting in a net loss of 3-hydroxyproline in fibrillar collagen, thereby leading to the autosomal recessive OI disease phenotype mentioned above. In this report we characterize a novel mouse model system in which the P3H1 gene has been inactivated, to better understand the molecular mechanisms underlying the disease. We show that inactivation of the P3H1 gene in mice causes abnormalities in collagen fibril ultrastructure in multiple tissues, including bone, tendon, and skin. These abnormalities are shown to be due to the loss of 3-hydroxyproline from key sites in collagen extracted from tissues, as well as due to the loss of the functions of the P3H1·CRTAP·CypB complex during active collagen biosynthesis. P3H1 therefore performs multiple roles during collagen biosynthesis and, when

* This work was supported by a grant from the Osteogenesis Imperfecta Foundation (to J. A. V.) and by grants from the Shriners Hospitals for Children (to H. P. B. and D. R. K.).

[S] The on-line version of this article (available at http://www.jbc.org) contains supplemental Fig. S1.

[1] To whom correspondence should be addressed: Shriners Hospital for Children, Research Dept., 3101 SW Sam Jackson Park Road, Portland, OR 97239. Tel.: 503-221-3433; Fax: 503-221-3451; E-mail: hpb@shcc.org.

[2] The abbreviations used are: OI, osteogenesis imperfecta; P3H1, prolyl 3-hydroxylase 1; CRTAP, cartilage-associated protein; CypB, cyclophilin B; WT, wild type.

absent, has a severe effect on bone formation and tissue integrity of those tissues containing predominantly fibrillar collagen.

EXPERIMENTAL PROCEDURES

P3H1 Null Mice—P3H1 null mice were purchased from Deltagen (San Mateo, CA). Directed knockouts were created in which exons 1–3 (nucleotides 15–817) of the mouse P3H1 or leprecan 1 gene (NCBI Reference sequence number: NM_019782.2) were deleted. Then a LacZ-Neo cassette was inserted into the area of the target gene that was deleted. P3H1 or leprecan gene inactivation was verified in mice by RNA preparation from tissues of null mice, followed by reverse transcription and PCR with primer sets spanning the length of the target gene. No P3H1 transcripts and gene expression were detected, as compared with normal levels of the target gene expressed in wild-type animals. Mice were bred multiple generations into a C57B6 background prior to analysis to verify phenotype effects, and data reported are from the fifth to eighth generations.

X-ray Scans and Bone Mineral Density—X-rays were performed on adult mice using a Faxitron cabinet instrument (model #43855B) made by Hewlett Packard. Voltages and exposure times were optimized for best resolution images.

Bone mineral measurements were performed by dual energy x-ray absorptiometry using the PIXImus instrument (Lunar Corp., Madison, WI). Densitometric analysis of the whole body (defined as the whole body image minus the calvarium, mandible, and teeth) was performed on freshly sacrificed mice. Food was withheld the night prior to sacrifice (to eliminate confounding effects of undigested rodent chow on bone mineral density assessment), and the mice were euthanized by CO_2 inhalation. The animals were weighed to the nearest 0.1 g and immediately underwent dual energy x-ray absorptiometry scanning. Then the left femora were harvested, wrapped in sterile gauze soaked in phosphate-buffered saline, and stored frozen at ≤ -20 °C for subsequent analyses.

Cortical femoral shaft bone geometry was examined by a desktop x-ray microtomographic scanner (SkyScan Model 1074, Aartselaar, Belgium). For image acquisition the specimen was mounted on a turntable to allow for three-dimensional imaging with a scan width of 17 μm. Images were stored in three-dimensional arrays and subsequently analyzed with Optimas software (version 6.2, Media Cybernetics, Silver Spring, MD).

To determine femoral structural properties, the left femur was tested to failure in three-point bending on a high resolution materials test apparatus (Model 4442, Instron Corp., Canton, MA). The loading fixture consisted of two fixed lower supports, placed at a span length of ~7-mm, and an upper loading point attached to a moving actuator. The femur was placed with its posterior surface resting on the two lower supports. The upper loading point contacted the specimen at its midpoint, which was coincident with the center of the span. System software was used to displace the actuator at a strain rate of 0.5%/s until failure occurred. Load and displacement data were recorded, and failure load and stiffness (calculated from the linear portion of the load *versus* displacement curve) were determined using system software.

Electron Microscopy Analysis of Tendon and Skin—Freshly obtained tissues were fixed in cacodylate-buffered 1.5% glutaraldehye/1.5% paraformaldehyde containing 0.05% tannic acid (w/v), then rinsed, exposed to 1% osmium tetroxide, then dehydrated in a grade series of ethanol to 100%. Fixed tissues were rinsed in propylene oxide and infiltrated and embedded in Spurr's epoxy. 80-nm ultrathin sections were mounted on Formvar-coated single hole slot grids and stained in ethanolic uranyl acetate followed by Reynold's lead citrate. Stained sections were examined using an FEI Tecnai G2 electron microscope operated at 120 kV and photographed using either an FEI Eagle 2K camera or an AMT 2K camera. Magnifications were calibrated using a grating replica (Ted Pella catalogue #603). The tomography tilt series was acquired from a 350 nm thick section at a magnification of 29,000× using an FEI Tecnai G2 transmission electron microscope operated at 200 KV. The micrographs were recorded automatically using a bottom mounted FEI Eagle 2K charge-coupled device camera. The micrographs were taken in a tilt range with a 2° increment from 40° to +40° and a 1° increment from −40° to −60° and from +40 to +65°. Images were aligned using FEI Inspect-3D software.

Skeleton Preparation—Skeletal preparations were followed as previously described (15) with the following changes. Briefly, pups were transferred to 50-ml tubes and frozen until ready to use, and then thawed and skin and internal organs up to the diaphragm were removed. Skeletons were fixed in 95% ethanol for 2 days, and lipids were subsequently removed in acetone for 2 days. Skeletons were then returned to 95% ethanol and soaked overnight and then stained for 10 days at 37 °C in 0.015 g of Alcian Blue 8GX, 0.005 g of Alizarin Red S, 5 ml of acetic acid, 75 ml of 95% ethanol, 20 ml of water. Stain was then replaced with distilled water, and skeletons were incubated for ~30 min, and then rinsed with one change of water. Clearing was started by placing skeletons in 30% saturated sodium borate (borax), 1% trypsin (cell culture grade), and digesting at 37 °C for 4–6 h. Skeletons were transferred to 1% KOH, 20% glycerol and incubated at room temperature until cleared (2–3 weeks). Skeletons were gradually transferred to 100% glycerol through 1% KOH, 50% glycerol and then 1% KOH, 80% glycerol, allowing a few days in each until finally stored in glycerol.

Mouse Tissue Histology—The following stain kits were purchased from Fisher Scientific: Von Kossa Stain kit for mineralized tissues, the Shandon Rapid-Chrome Frozen Section Staining kit from Thermo Scientific for hematoxylin and eosin staining of nuclei and cytoplasmic and extracellular protein stain, and the Masson Trichrome Staining kit for differentiating collagen from smooth muscle in tissue samples. Staining for all kits was performed according to the manufacturer's instructions.

Collagen Extraction from Tissues—Tendons were extracted from adult mouse tails and pepsinized in 0.5 M acetic acid. Briefly, tendons were incubated at 4 °C in excess volumes of 0.5 M acetic acid with shaking for several hours. Pepsin was added to a final concentration of ~1 mg/ml, and tendons were digested at 4 °C overnight. Solution was centrifuged to remove insoluble material, then NaCl was added to a final concentration of 0.7 M to precipitate collagen, and solution was incubated

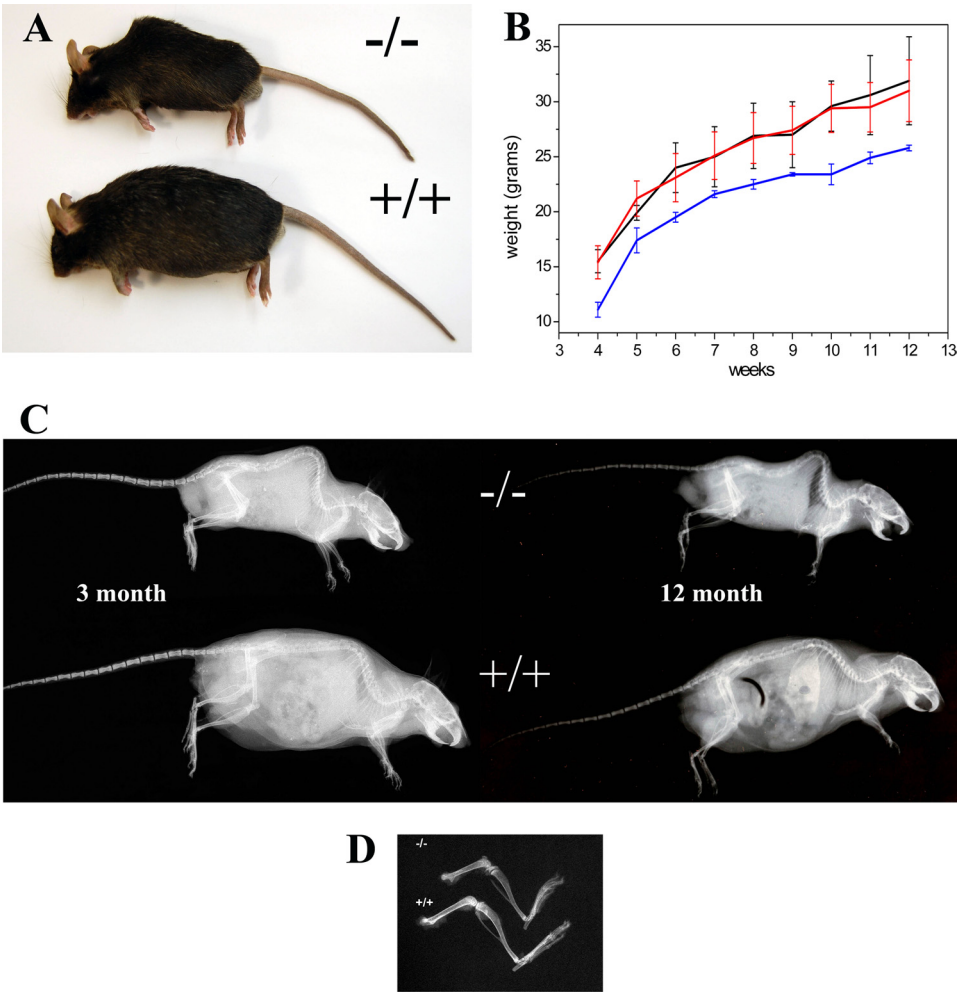

FIGURE 1. **Reduced body size and x-ray analysis of mice.** P3H1 knock-out mice typically appear smaller in size (*A*). Wild-types (*B*, *black curve*), heterozygotes (*B*, *red curve*), and homozygotes (*B*, *blue curve*) weights are plotted as a function of age with standard deviations shown. Null mice are considerably smaller already at 3 weeks of age and stay smaller through the lifetime. Full body x-rays (*C*) show pronounced curvature of the vertebrae and thinner skull of knock-out mice as compared with age- and sex-matched wild-type mice. The difference is obvious at 3 month age but progresses further in life as seen in the x-rays of 12 month old mice (*C*, *right side*). Hind limb x-rays (*D*) of P3H1 null mice show decreased bone mineral density as well as a foreshortening of the proximal bone relative to the distal bone in comparison with wild-type hind limb.

TABLE 1
Ratios of proximal to distal bone lengths

	Femurs	Tibias	Ratio
	mm	*mm*	%
Wild type mice[a]	14.90 ± 0.3	18.70 ± 0.7	79.8
P3H1 null mice[a]	12.00 ± 0.6	18.27 ± 0.4	66.7

[a] Age- and sex-matched adult mice ($n = 10$), $p < 0.0001$.

TABLE 2
Whole body phenotype of adult mice

Values are mean ± S.D., $n = 8$, 20-week-old and sex-matched mice. Differences between null and wild type are statistically significant ($p < 0.01$). Differences between wild-type and heterozygous mice are not statistically significant.

	Wild types	Heterozygotes	P3H1 nulls
Weight (g)	37.94 ± 4.55	37.56 ± 3.86	25.81 ± 3.63
Whole body bone mineral density	55.66 ± 4.21	55.59 ± 1.71	48.87 ± 2.13
Whole body % Fat	27.85 ± 3.67	28.28 ± 6.16	19.29 ± 3.63

at 4 °C 2–4 h. Precipitate was collected by centrifugation at 20,000 × *g* for 40 min and resuspended in 0.1 N acetic acid. Saturated Tris was added to bring collagen solution to neutral pH, and then NaCl was added to a final concentration of 2.5 M NaCl to preferentially precipitate type I collagen. Solution was incubated at 4 °C for several hours and then centrifuged at 20,000 × *g* for 40 min to collect the collagen precipitate. Pellet was resolubilized in 0.1 M acetic acid, analyzed on SDS-PAGE gels, and lyophilized for further digestion and analysis.

Collagen Digestion and MS Analysis—Pepsinized collagen was resuspended in 70% formic acid and digested overnight at room temperature with cyanogen bromide (Sigma) to generate fragments for further analysis. The digested solution was lyophilized and then subjected to sieve chromatography on tandem Superose 12 columns using the AKTA fplc system (Amersham Biosciences) to separate the fragments in 0.1 M sodium acetate buffer, pH 4.5. The appropriate cyanogen bromide peptide containing the putative 3-hydroxyproline site was selected based on fragment size and time of elution and was subjected to further digestion with sequencing grade trypsin (Promega, Madison, WI) in 100 mM ammonium bicarbonate at 37 °C overnight. Additionally, tendon extracted and pepsinized type I collagen was run on one-dimensional SDS-PAGE, and the α1(I) and α2(I) gel bands were subjected to in-gel digestion with trypsin using a protocol similar to that described by Shevchenko *et al.* (16). Digestion conditions were 13 ng/μl of sequencing grade trypsin (Promega) in 100 mM ammonium bicarbonate at 37 °C for 18 h. Prior to analysis, digested proteins were desalted and purified using C18 SPE columns. Liquid chromatography-tandem mass spectrometry was performed on a Waters Q-TOF Micro mass spectrometer with a LockSpray electrospray ionization source coupled to a Waters CapLC high-performance liquid chromatography system. Chromatographic separation took place by gradient elution using a 75-μm × 100-mm, 3-μm Atlantis dC18 analytical column. Tryptic peptides were identified from all tandem mass spectrometry spectra by a Mascot search (Matrixscience) against the NCBI nonredundant data base.

Secretion Rate Assay—Primary mouse skin fibroblasts at early passage number (P1) were grown to confluence, trypsinized, and counted. Cells were adjusted to equalize cell number across different cell types and then resuspended in serum-free medium and recounted. Cells were preincubated in labeling medium (methionine-free Dulbecco's modified Eagle's

TABLE 3
Structural properties of femoral bone of 20-week-old mice

	Wild types	Heterozygotes	P3H1 nulls	*p* value[a]
Length	16.57 ± 0.35	16.36 ± 0.29	15.11 ± 0.10	<0.0001
Bone density	63.1 ± 6.8	62.8 ± 3.1	54.3 ± 3.5	<0.01
Cortical area	0.819 ± 0.079	0.799 ± 0.058	0.768 ± 0.062	NS
Cortical thickness	0.171 ± 0.01	0.174 ± 0.009	0.160 ± 0.011	<0.01
Force to failure (newtons)	22.79 ± 2.82	23.87 ± 2.19	19.92 ± 4.23	<0.05
Stiffness (newtons/mm)	108.44 ± 8.75	117.11 ± 8.71	95.51 ± 10.42	<0.01

[a] Statistical analysis Student's *t*-test comparing P3H1 nulls with combined data from wild-type and heterozygote animals (NS is not significant).

medium without fetal bovine serum but with ascorbate at a final concentration of 50 μg/ml at 37 °C with gentle shaking for at least 20 min). Cells were briefly centrifuged, and medium was removed and replaced with 10 ml of labeling medium containing 1 mCi of [2,3,4,5-^{3}H]proline (90 Ci/mmol) and 1 mCi [^{35}S]methionine (1175 Ci/mmol) and incubated with shaking at 37 °C for 30 min. Cells were then spun out briefly and resuspended in chase medium (standard Dulbecco's modified Eagle's medium with cold methionine and ascorbate) and aliquoted for separate time points (*i.e.* 0 min, 15 min, 30 min, 60 min, and 2 h). Cells were incubated at 37 °C with shaking, removed at each time point, and spun out at high speed. Medium was transferred to labeled fresh tube, and cell pellet and medium were frozen. After thawing 1 ml of lysis buffer (1% Nonidet P-40 and 10 mM EDTA in phosphate-buffered saline) was added to each cell pellet and mix. Cell lysates and medium were precipitated with ammonium sulfate (200 mg per 1 ml of volume was added to each tube, incubated 2–3 h with shaking at 4 °C.) Precipitates were centrifuged at high speed for 20–30 min at 4 °C and the resultant pellet was resuspended in 0.5 M acetic acid with 0.4 mg/ml pepsin. Samples were digested overnight at 4 °C with shaking. Pepsinized collagen extracts were precipitated with 0.7 M NaCl final concentration at 4 °C and spun out at high speed for 30 min. Pellets were resuspended in 0.5 M acetic acid and SDS-PAGE sample buffer, run on 6–8% acrylamide gels, dried, and exposed to film for autoradiography.

Amino Acid Analysis—Acid hydrolysis was performed in 6 × 50 mm Pyrex culture tubes placed in Pico Tag reaction vessels fitted with a sealable cap (Eldex Laboratories, Inc., Napa, CA). Samples were placed in culture tubes, dried in a SpeedVac (GMI, Inc., Albertsville, MN), and then placed into a reaction vessel, which contained 250 ml of 6 N HCl (Pierce) containing 2% phenol (Sigma-Aldrich, Milwaukee, WI). The vessel was then purged with argon gas and vacuumed using an automated evacuation Hydrolysis/Derivatization workstation (Eldex Laboratories, Inc., Napa, CA). Closing the valve on the Pico Tag cap maintains the vacuum during hydrolysis at 110 °C for 24 h. The hydrolyzed samples were then dried in a Savant SpeedVac. The dried samples were dissolved in 100 ml of 0.02 N HCl containing an internal standard (100 micro M norvaline, Sigma). Appropriate further dilutions were made using the same dilution solvent for concentrated samples. Analysis was performed by ion exchange chromatography with postcolumn ninhydrin derivatization and visible detection (440 nm/570 nm) with an Hitachi L-8800A amino acid analyzer (Hitachi High Technologies America, Inc., San Jose, CA) running EZChrom Elite software (Scientific Software, Inc., Pleasanton, CA).

Base hydrolysis was performed in 1.7-ml polypropylene tubes placed in Pico Tag reaction vessels fitted with a sealable cap. Lyophilized protein samples of ~0.8 mg for each were suspended in 100 ml of 1 N NaOH. The vessel was purged with argon gas and vacuumed as above. The vessels were kept at 110 °C for 24 h. The hydrolyzed sample was cooled down, and the 800 μl of water was added, followed by the addition of 2 N HCl to neutralize the solution. The sample solution 50 μl, 50 μl of 0.2 M borate buffer, pH 9.5, and 50 ml of 10 mM 4-fluoro-7-nitrobenzofurazan (CAS# 29270-56-2, Dojindo, Rockville, MD) in acetonitrile were mixed and kept at room temperature for 4–6 h, followed by the addition of 100 μl of tartrate buffer, pH 2.0. The 7-nitro-1,2,3-benzoxadiazole labeled amino acids were analyzed by the precolumn labeled method (17) with a small modification. Cadenza CD-C18 (250 × 4.6 mm, inner diameter, 3 μm, Imtakt Co., Kyoto, Japan) column was used for the separation of the labeled amino acids. A Gilson Model 121 fluorometer (Middleton, WI) with two filters from Andover Corp. (Salem, NH); edge filter short wave pass 450FL07-25, and the standard bandpass filter 530FS10-12.5 were used as the excitation and the emission filters, respectively. The eluted peak analysis was performed with MassLynx software (Waters).

Circular Dichroism—Circular dichroism spectra were recorded on an AVIV 202 spectropolarimeter (AVIV Biomedical, Inc., Lakewood, NJ) using a Peltier thermostatted cell holder and a 1-mm path length rectangular quartz cell (Starna Cells Inc., Atascadero, CA). Collagen samples were dissolved in 50 mM Tris-HCl, pH 7.5, containing 10% (v/v) glycerol. The temperature-scanning experiments were at 10 K/h. The ellipticity at 221 nm was monitored as a function of time.

RESULTS

P3H1 Null Mice Are Smaller, Grow Slower, and Have Bone Defects—Heterozygous P3H1 mice do not have an observable phenotype. The P3H1 null mice are fertile and viable. P3H1 null and wild-type littermates were weighed weekly from 3 to 20 weeks of age to measure their growth rate. P3H1 null mice are significantly smaller and never reach the size of their wild-type and heterozygous littermates, even after reaching adulthood (Fig. 1, *A* and *B*). P3H1 mice develop kyphoscoliosis (Fig. 1*C*), which gets progressively worse with age. Bone density in the skull, as well as in the limbs (Fig. 1*D*), is also decreased in the P3H1 null mice as compared with their wild-type littermates. The delay in their postnatal growth is characterized by shortening of the long bone segments. More specifically, hind limbs were analyzed to determine differences in the femoral *versus* the tibial lengths in P3H1 null *versus* wild-type mice (Table 1). Rhizomelia is evident in the P3H1 null mice as measured by a significant decrease in the ratio of the femoral length to the tibial length (Table 1) by ~16%. Bone defects are also apparent

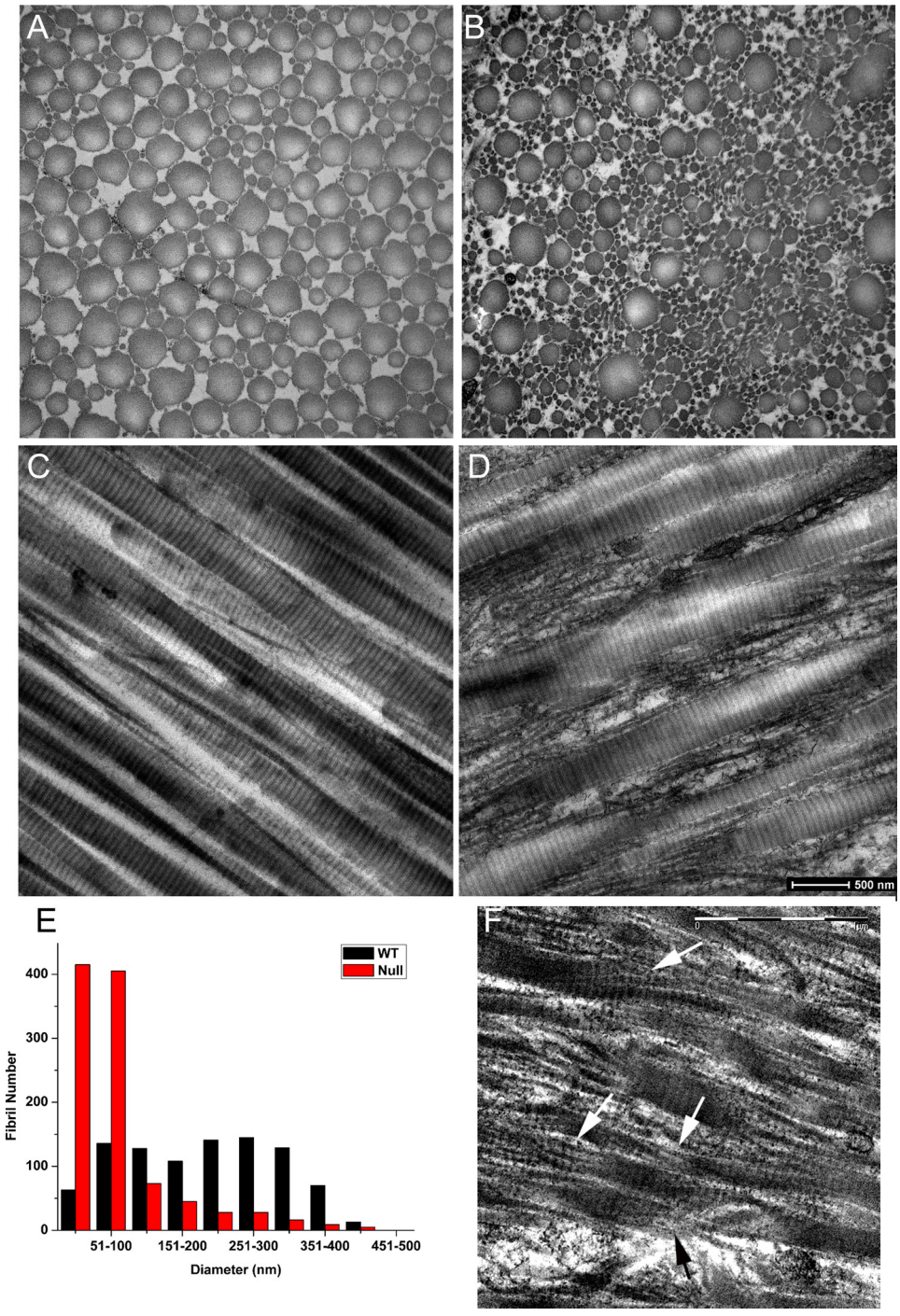

FIGURE 2. **Tendon fibrils of P3H1 null mice compared with wt mice.** Electron microscope images of tail tendon fibrils from adult wild-type (*A* and *C*) and adult P3H1 null mice (*B* and *D*). Cross-sections of the collagen fibrils (*A* and *B*) show a more heterogeneous distribution of fibril diameters as well as some disturbances in the overall shape of some of the fibrils in the P3H1 null mice as compared with the wild-type fibrils. Longitudinal sections of the tendon collagen fibrils (*C* and *D*) show an alternating pattern of very small fibrils interspersed with very large fibrils as well as abnormal branching at the ends of some of the P3H1 null fibrils as compared with the wild-type fibrils. (*Scale bar* in *D* represents 500 nm and is the same for images *A–D*.) Tendon fibril size *versus* number of fibrils measured was *graphed* (*E*) and demonstrates a shift in the size distribution from 100 nm to 350 nm in the wild-type to primarily 0–100 nm in the null ($n = 1000$ for wt and $n = 1000$ for P3H1 null). *F*, a projection through a 350 nm thick section of longitudinally sectioned P3H1 null tendon from which the tomogram (supplemental Fig. S1) was collected. *Arrows* point to regions in the tendon in which thicker fibrils branch into thinner fibrils and where axial twists are evident.

by dual energy x-ray absorptiometry or micro-computed tomography scans performed on wild-type, heterozygous, and P3H1 null mice at 20 weeks of age (Table 2). Whole body bone mineral density of the P3H1 null mice was decreased by ~12.5% in comparison with the bone mineral density of the wild-type mice. Femoral bone mineral density, as well as femoral length, were also determined to be significantly lower in the P3H1 null mice in comparison to age- and sex-matched wild-type mice (Table 3). Bone mineral density differences between wild-type and heterozygous mice were not statistically significant. P3H1 null mice also show a significant decrease in body fat (Table 2). The stiffness and the force to failure of the femurs of 20-week-old P3H1 null mice were significantly lower as compared with heterozygous and wild-type mice (Table 3).

Tendons of P3H1 Mice Have Abnormal Morphology—Transmission electron microscopy images were taken of tail tendons from wild-type and P3H1 null mice (Fig. 2). P3H1 null tendons show acute ultrastructural defects in overall shape and diameter as compared with wild-type tendons (Fig. 2, *A–D*). Cross-section images of P3H1 null tendons demonstrate a large increase in the number of small diameter fibrils (Fig. 2, *A* and *B*). Longitudinal sections of P3H1 null mouse tail tendons reveal heterogeneity in overall fibril contour as compared with age-matched wild-type tail tendons (Fig. 2, *C* and *D*). There is also an axial twist noted in many of the longitudinally sectioned P3H1 null tendon collagen fibrils, seen to best advantage in the tomogram (supplemental Fig. S1). Furthermore, larger collagen fibrils within the P3H1 null tendons appear to branch into numerous smaller diameter fibrils (Fig. 2*D*), again seen to best advantage in the tomogram (supplemental Fig. S1). Fibril diameters of tail tendon collagen fibrils were measured and graphed as a function of number. P3H1 null mouse tendon fibrils show an altered distribution of fibril sizes in which the large majority are between 20 and 100 nm as compared with a more even distribution of fibrils across a much broader range of diameters (50–400 nm) in the wild-type mouse tendons (Fig. 2*E*). Tendon cells

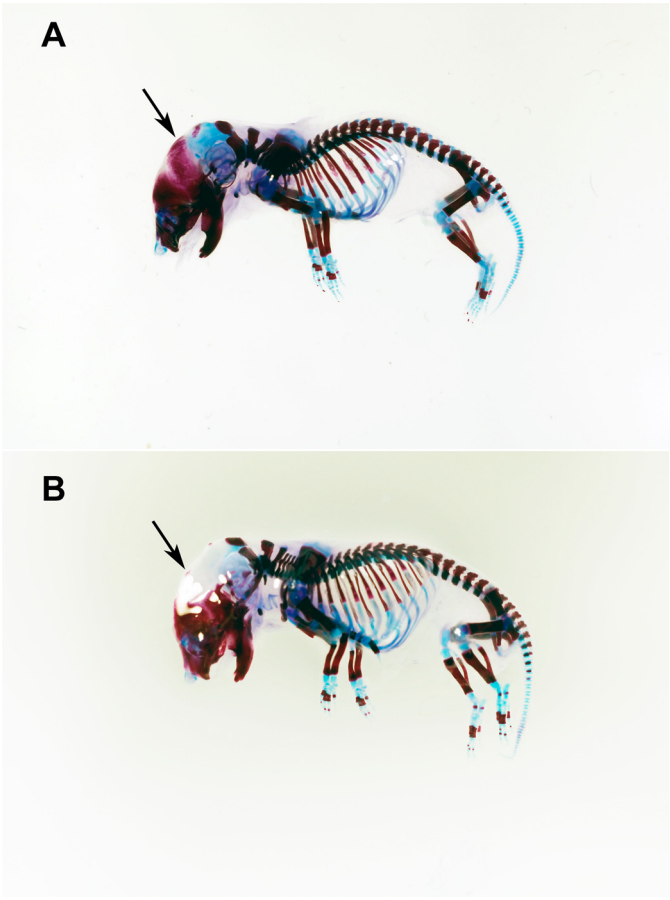

FIGURE 3. **Skeleton preparations of E18 mice.** Skeletons of E18 mice were stained with alizarin red and Alcian blue to detect differences in mineralized bone and cartilage, respectively (*A* and *B*). The primary difference detected at this developmental stage is the lack of ossification in the parietal bone in the skull of null mice (*B*) as compared with heterozygous mice (*A*) indicating a delay in ossification in the P3H1 null mice. (Note: bone mineral density in heterozygous mice was indistinguishable from that of wild-type mice (see Table 2)).

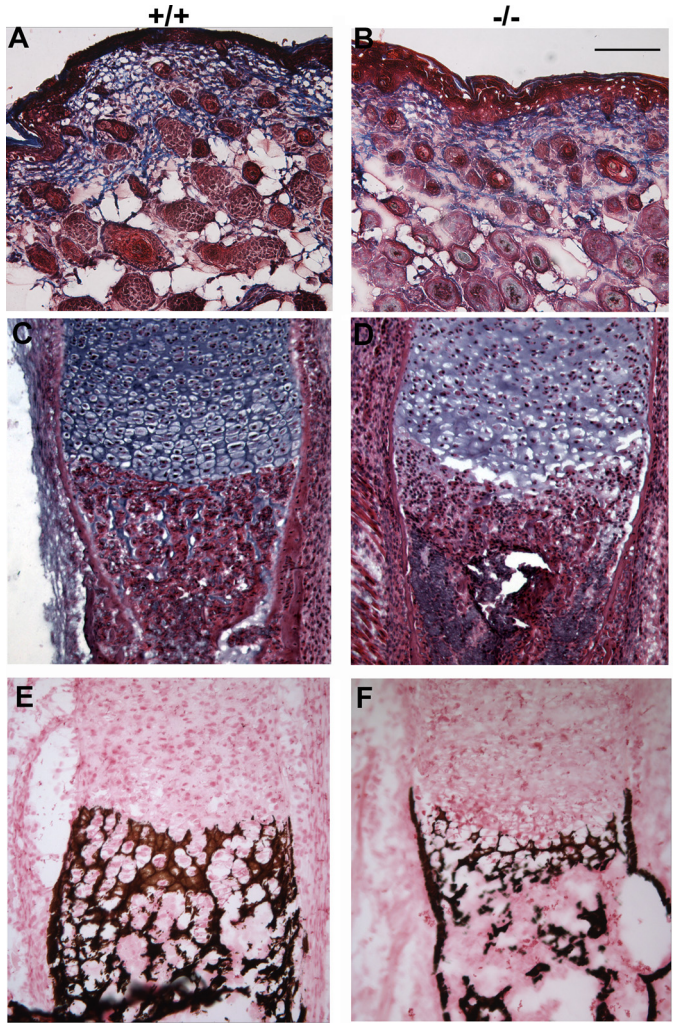

FIGURE 4. **Histochemistry of hind limbs.** Newborn (P0) hind limbs were cryosectioned and stained with Masson trichrome stain to detect collagen fibrils (*blue*) in skin of wild-type (*A*) and P3H1 null mice (*B*). Collagen fibril staining in the skin of newborn null mice was less intense and less dense suggesting an overall decrease in the amount of collagen in the dermis. Sections of P1 fore limbs were also stained with hematoxylin and eosin to look at the overall organization of the chondrocytes in wild-type (*C*) and null (*D*) radial cartilage. The hypertropic zone in the P3H1 null limb (*D*) appears to be severely affected compared with the same region in the wild-type limb (*C*). Newborn hind limb sections were also stained with Von Kossa stain to detect mineralized bone (*E* and *F*). P3H1 null femurs (*F*) have less mineralized bone in the trabeculae with more spaces throughout as compared with wild-type femurs (*scale bar* = 120 μm).

from P3H1 null mouse tails were also analyzed by electron microscopy and determined to have structural abnormalities in terms of a decrease in the number and length of cell processes as compared with wild-type tendons (data not shown). Fig. 2*F* shows a projection through a 350 nm thick section of longitudinally sectioned P3H1 null tendon from which the tomogram was collected.

Staining of E18 Skeletons Shows Delay in Ossification—E18 skeletons of heterozygous (Fig. 3*A*) and P3H1 null (Fig. 3*B*) mice were stained with alizarin red (to detect bone) and Alcian blue (to detect cartilage). The P3H1 null skeletons show a lack of staining in the parietal bone of the skull indicating a delay in ossification in this area. Other elements of the skeleton looked relatively normal at this stage of development.

Histology of Newborn and Adult Limb Sections Shows Disturbances in Morphology—Cryosections of newborn limbs were stained for collagen with Masson trichrome blue stain (Fig. 4, *A* and *B*). P3H1 null skin (Fig. 4*B*) has less overall blue staining indicating a less densely packed dermis with less collagen fibrils present as compared with the wild-type skin (Fig. 4*A*). P1 fore limbs were also sectioned and stained with hematoxylin and eosin to compare differences in cartilaginous elements of the radius (Fig. 4, *C* and *D*). P3H1 null chondrocytes (Fig. 4*D*) in the hypertrophic zone appear to be less organized than those in the same region in the wild-type limb cartilage (Fig. 4*C*). Finally, newborn hind limb sections were stained with Von Kossa stain to detect mineralized bone (Fig. 4, *E* and *F*). P3H1 null femurs (Fig. 4*F*) have significantly less mineralized bone in the trabecular area with more spaces interspersed throughout suggesting less density overall as compared with the wild-type femurs (Fig. 4*E*). This observation is in good agreement with the femoral dual energy x-ray absorptiometry (DEXA) and micro-computed tomography studies (Table 3) that demonstrate reduced bone mineral density and cortical thickness of P3H1 null femora. Adult mouse skin sections were stained with Masson trichrome stain to look at collagen differences between wild-type and P3H1 null mice (Fig. 5, *E* and *F*). Although there was a

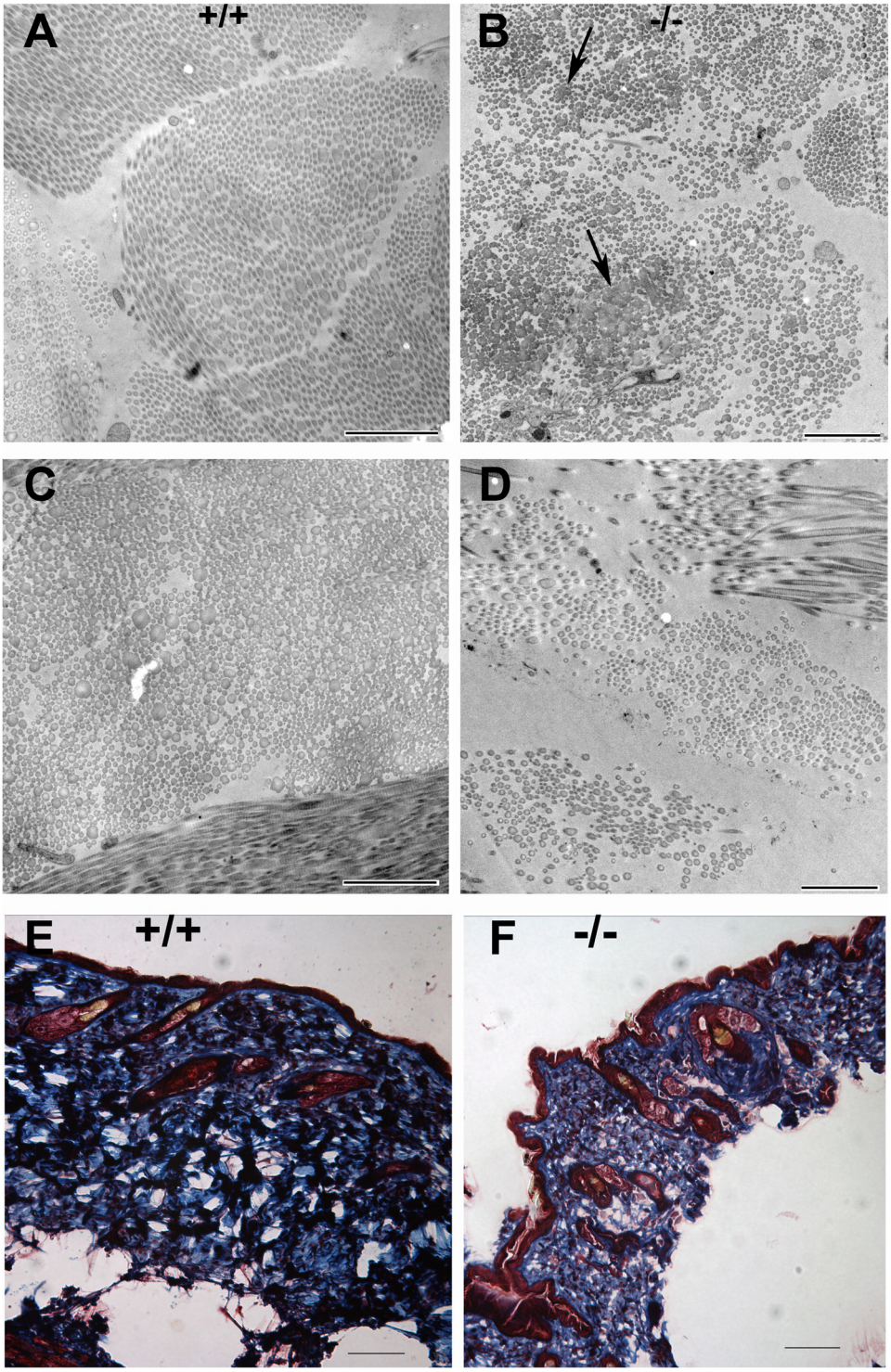

FIGURE 5. **Skin of P3H1 null mice.** Electron microscope images of adult wild-type (*A* and *C*) and P3H1 null mouse skin (*B* and *D*) were analyzed and show abnormalities in the reticular dermis of the null skin collagen fibrils where many irregular, fused collagen fibrils are found (*arrows* in *B*), as well as more spaces between fibril bundles (*D*) as compared with wild-type skin (*scale bar* = 2 μm). Cryosections of adult skin were also stained with Masson trichrome stain to detect collagen fibrils in wild-type (*E*) and null (*F*) dermis (*scale bar* = 120 μm). P3H1 null skin was overall thinner and slightly less dense than the wild-type skin.

similar intensity of blue staining, indicating similar amounts of collagen present in the dermis, the null skin (Fig. 5*F*) was much thinner than the wild type (Fig. 5*E*). Adult mouse skin from wild-type and null mice was also analyzed by electron microscopy (Fig. 5, *A* and *B*). Abnormalities are present in the reticular dermis of the null mice where bundles of relatively normal looking fibrils are interspersed with clumped areas of collagen fibrils (Fig. 5*B*) and some gaps and spaces in between collagen fibrils (Fig. 5*D*) that are not present in the wild-type skin.

Collagen Extracted from P3H1 Mice Shows Differences from Wild-type Collagen—Type I collagen was extracted from the tendons of wild-type and P3H1 null mice and analyzed by SDS-PAGE. Slight differences in the gel mobility of the α1 and α2 chains were seen indicating overmodification of the collagen (Fig. 6*A*). Extracted collagen from the mice tendon was also subjected to trypsin digestion and analysis by mass spectrometry to identify the peptide containing the single 3-hydroxyproline, Pro-986 in the wild-type mouse collagen. As expected the tryptic fragment from type I collagen of P3H1 null mice was lacking the 3-hydroxyproline as compared with the same fragment from the wild-type mice, which contained the appropriate 3-hydroxyproline residue (Fig. 6*B*). The type I collagen extracted from wild-type and P3H1 null mice was also analyzed by amino acid analysis to determine the overall levels of 4-hydroxyproline and hydroxylysine. Table 4 shows the results in which the P3H1 null mouse tendon type I collagen was determined to have a slight increase in the percentage of 4-hydroxylation as compared with type I collagen from wild-type mice. A much more significant increase was seen in the percentage of lysyl hydroxylation in the P3H1 null mouse collagen I (22.5%) as compared with that from wild-type mice (17.8%) (Table 4). An analysis of base-hydrolyzed type I collagen from tail tendon, bone, and skin of normal and wild-type tissue indicates a remarkable increase in glucosyl galactosyl hydroxylysine (Table 5). The highest amount of this modification was found in bone. The increase in 4-hydroxyproline and glycosylation leads to a slight increase in the melting temperature of type I collagen extracted from mutant tail tendons as compared with wild-type collagen (Fig. 7).

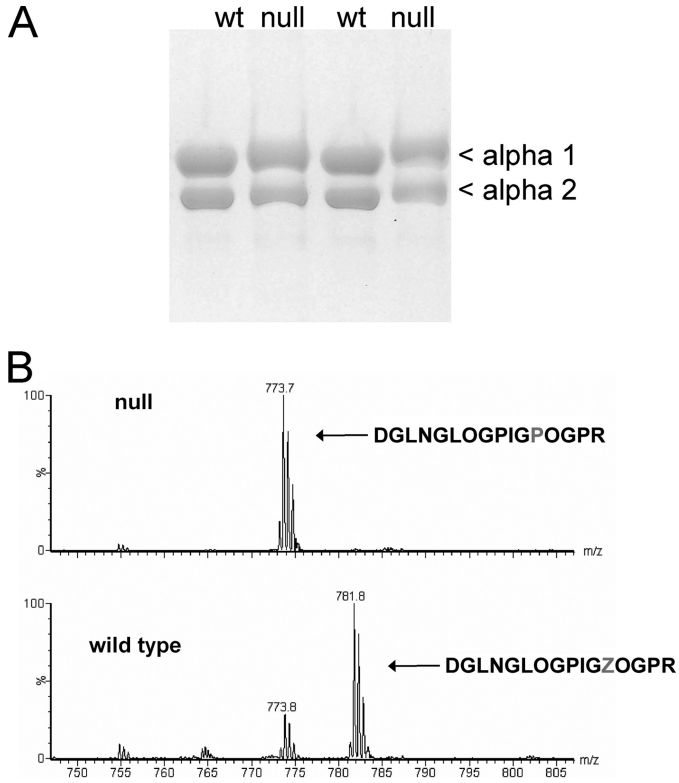

FIGURE 6. **3-hydroxyproline in wt and P3H1 null mice.** SDS-PAGE of extracted and pepsin digested wild-type and P3H1 null collagen I from tail tendon (*A*) shows a mobility shift in P3H1 null collagen as compared with wild-type indicating overmodified collagen molecules. Mass spectrometry data (*B*) of the trypsin fragment containing the single 3-hydroxyproline site in the alpha 1 chain of collagen I show the presence of 3-hydroxyproline at proline 986 in the wild type, but it is not present at the same location in the P3H1 null mouse collagen. *O*, 4(*R*)-hydroxyproline; *Z*, 3(*S*)-hydroxyproline in the indicated sequences.

TABLE 4

Amino acid composition of type I collagen extracted from mouse tail tendons (acid hydrolysis)

	4Hyp/(Pro+4Hyp)[a]	Estimated number of 4Hyp residues	4Hyp experimental/possible maximum[b]
Null	0.464	306	0.937 (306/327)
WT	0.450	297	0.909 (297/327)
Difference	0.014	9	
cf. Human placenta	0.463	313	0.951 (313/329)
	Hyl/(Lys+Hyl)[a]	**Estimated number of Hyl residues**	**Hyl experimental/possible maximum[a]**
Null	0.225	23.2	0.331 (23.2/70)
WT	0.178	18.3	0.262 (18.3/70)
Difference	0.047	4.9	

[a] Values are averaged from experimentally determined amino acid compositions done in triplicates at each of three different dilutions.
[b] Experimental value was divided by the calculated Pro residues in the Y position (327).

TABLE 5

Amino acid analysis of type I collagen from different normal and mutant mouse tissues (base hydrolysis)

	Hyl/(Hyl+Lys)	Hyl/(Hyl+Lys) null/WT	Glucosyl galactosyl hydroxylysine ratio null/WT
Tendon WT	0.15		
Tendon null	0.16	1.08	1.28
Bone WT	0.19		
Bone null	0.26	1.42	2.40
Skin WT	0.11		
Skin null	0.15	1.32	1.49

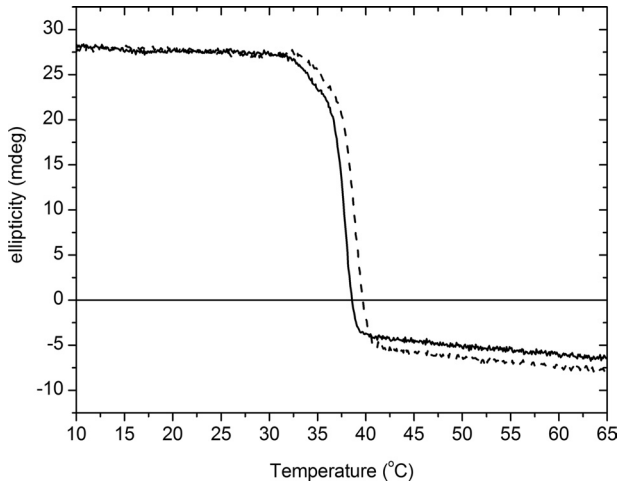

FIGURE 7. **Thermal stability of type I collagen.** Temperature scan of type I collagen extracted from mutant and wild-type tail tendons. The circular dichroism signal was monitored at 221 nm, and the rate of heating was 10 °C/h. The curves for wild-type (*solid line*) and mutant (*dashed line*) type I collagen are shown.

Collagen Secretion Rate Is Decreased in P3H1 Null Fibroblasts—The rate of collagen secretion in wild-type and null primary mouse skin fibroblasts was measured. The rate of secretion is delayed in the null mouse skin fibroblasts as compared with wild-type skin fibroblasts (Fig. 8). The level of type I collagen synthesized from P3H1 null mouse skin fibroblasts is ~70% of the level from wild-type mice fibroblasts. This ratio is roughly consistent with the amount of collagen precipitated from wild-type and null mouse tendon after pepsin extraction, when starting with the same wet weight of tissues.

DISCUSSION

Prolyl 3-hydroxylase 1 has been shown to be crucial for proper bone formation as human mutations result in a severe recessive bone disorder that resembles osteogenesis imperfecta (5–6, 10). Here we describe a mouse model in which the P3H1 gene has been inactivated in mice. We show that loss of P3H1 in mice causes a bone disorder that is characterized by a decrease in overall bone density, kyphosis, rhizomelia, as well as a delay in ossification in some bones in the developing null mice. Although the observed phenotypes in CRTAP null mice and human mutations in CRTAP and P3H1 have been shown previously to primarily affect bone, we show here that, in addition to defects in bone, loss of P3H1 in mice causes disturbances in other fibrillar collagen-rich tissues such as tendons and skin. This was also found for the CypB null mice (11). In these tissues the collagen fibril distribution and packing are affected and the overall amount of extractable collagen is severely reduced in the P3H1 null mice. It is interesting to note here that decorin and biglycan knock-out mice have also been shown to have disturbances in their collagen fibril morphology in skin, tendon, and bone suggesting a possible interaction site on the collagen that may be dependent on the presence of 3-hydroxyproline (18).

Bone and energy metabolism have been shown to be balanced with each other and are coregulated on a molecular basis through a common signaling pathway in the brain (19, 20). Our data show a significant decrease in total body fat in the P3H1

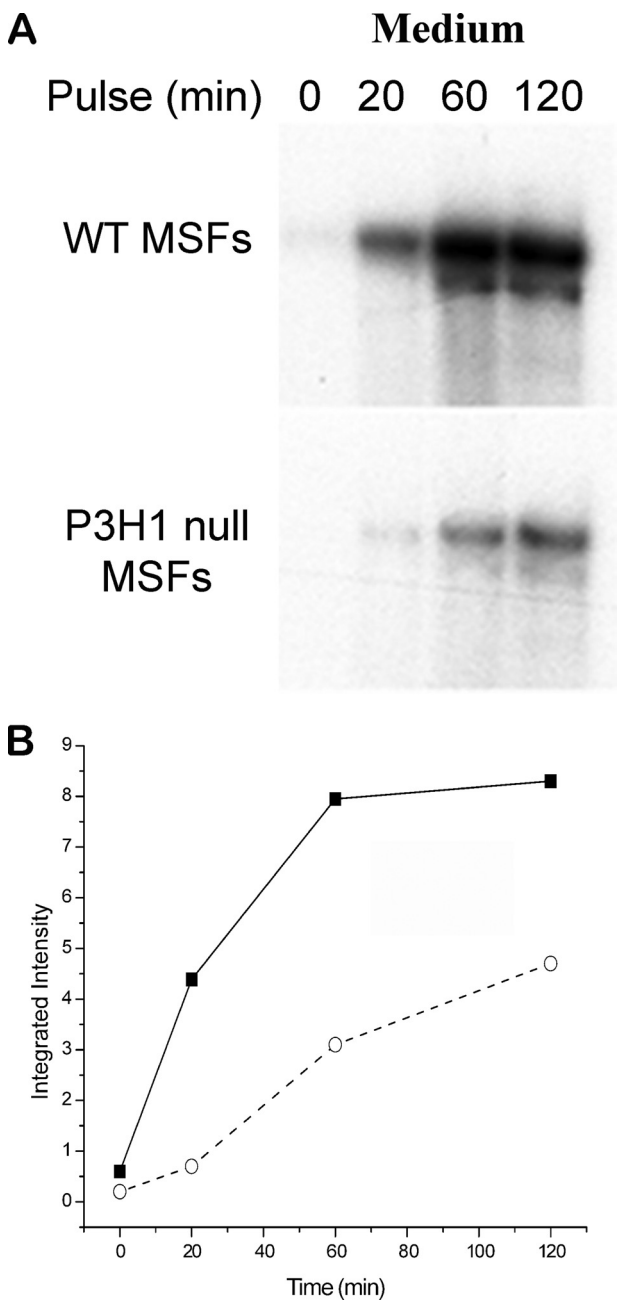

FIGURE 8. **Secretion of type I collagen.** Collagen secretion rate assay was performed using wild-type and P3H1 null primary mouse skin fibroblasts. Cell numbers were equalized prior to labeling, and results demonstrate a delay in collagen secretion in the null cells by at least 20 min and a lesser total amount of labeled collagen in P3H1 null fibroblasts. The secretion rate of type I collagen is represented *graphically* and shows maximal secretion at 60 min for the wild-type collagen (*solid line* with *filled square*) and 120 min for the null mouse collagen (*dotted line* with *open circle*).

null mice that have decreased bone mineral density. This could be related to the coordinated regulation of bone and energy metabolism, but further metabolic phenotyping studies would be required to delineate this effect.

3-Hydroxyproline is found in almost all collagens in the sequence -Gly-3Hyp-4Hyp-Gly- (21–23), however, the extent of 3-hydroxylation varies with the different types of collagens and occurs in the largest amounts in collagen types IV and V (13, 24–26). 3-Hydroxyproline occurs at a single site in the alpha I chain of type I collagen, at proline 986 (13). The *in vivo* function of a single 3-hydroxyproline residue in the triple helical domain of fibrillar collagen is still unclear, however, it was recently shown that, the conversion of a Pro to 3(*S*)-Hyp residue in the Xaa position of a Gly-Xaa-Yaa synthetic peptide slightly increases the stability of the triple helical structure (27). Recent observations on the existence of additional conserved 3-hydroxyproline sites, sequence motif, and spacing indicate a role for 3-hydroxyproline in the ordered self assembly of collagen supramolecular structures (13).

P3H1 forms a stable complex with CRTAP and CypB and the complex is now known to be important for both its enzymatic activity as well as for its chaperone effects on the newly forming collagen chain (12, 14). P3H1 null fibroblasts show a delay in collagen secretion suggesting that, in the absence of P3H1, the complex cannot form and results in a delay in collagen folding and secretion. Mobility shifts of the collagen molecules on SDS-PAGE gels, as well as overall amino acid compositions demonstrate an overmodification of collagen as a result of the delay in secretion. This appears to be primarily an excess of hydroxylysine, as well as an increase in the number of glucosyl galactosyl hydroxylysine per collagen molecule in the null mice. It is reasonable to suggest that the increase in sugar residues may cause packing problems in the assembly of collagen fibrils into higher ordered molecular weight structures. We also have noticed an increase in the cross-linking in the P3H null mouse collagen as obtained by acid hydrolysis *versus* base hydrolysis indicating the presence of acid labile cross-links that are not seen in base hydrolysis. Taken together these data suggest a combined effect in the P3H1 null mice whereby a delay in collagen secretion results in overmodified collagen molecules that may be incorrectly assembled into the extracellular matrix of collagen-rich tissues such as bone, tendon, and skin. This in turn has a severe effect on the ultimate form and function of these tissues.

Acknowledgment—We thank Ruggero Tenni for a sample of glucosyl galactosyl hydroxylysine.

REFERENCES

1. Sillence, D. O., Senn, A., and Danks, D. M. (1979) *J. Med. Genet.* **16,** 101–116
2. Rauch, F., and Glorieux, F. H. (2004) *Lancet* **363,** 1377–1385
3. Royce, P. M., and Steinmann, B. (eds) (2002) *Connective Tissue and Its Heritable Disorders: Molecular, Genetic, and Medical Aspects*, pp. 385–430, Wiley-Liss, New York
4. Morello, R., Bertin, T. K., Chen, Y., Hicks, J., Tonachini, L., Monticone, M., Castagnola, P., Rauch, F., Glorieux, F. H., Vranka, J., Bächinger, H. P., Pace, J. M., Schwarze, U., Byers, P. H., Weis, M., Fernandes, R. J., Eyre, D. R., Yao, Z., Boyce, B. F., and Lee, B. (2006) *Cell* **127,** 291–304
5. Baldridge, D., Schwarze, U., Morello, R., Lennington, J., Bertin, T. K., Pace, J. M., Pepin, M. G., Weis, M., Eyre, D. R., Walsh, J., Lambert, D., Green, A., Robinson, H., Michelson, M., Houge, G., Lindman, C., Martin, J., Ward, J., Lemyre, E., Mitchell, J. J., Krakow, D., Rimoin, D. L., Cohn, D. H., Byers, P. H., and Lee, B. (2008) *Hum. Mutat.* **29,** 1435–1442
6. Willaert, A., Malfait, F., Symoens, S., Gevaert, K., Kayserili, H., Megarbane, A., Mortier, G., Leroy, J. G., Coucke, P. J., and De Paepe, A. (2009) *J. Med. Genet.* **46,** 233–241
7. Barnes, A. M., Chang, W., Morello, R., Cabral, W. A., Weis, M., Eyre, D. R., Leikin, S., Makareeva, E., Kuznetsova, N., Uveges, T. E., Ashok, A., Flor, A. W., Mulvihill, J. J., Wilson, P. L., Sundaram, U. T., Lee, B., and Marini,

J. C. (2006) *N. Engl. J. Med.* **355,** 2757–2764
8. Cabral, W. A., Chang, W., Barnes, A. M., Weis, M., Scott, M. A., Leikin, S., Makareeva, E., Kuznetsova, N. V., Rosenbaum, K. N., Tifft, C. J., Bulas, D. I., Kozma, C., Smith, P. A., Eyre, D. R., and Marini, J. C. (2007) *Nat. Genet.* **39,** 359–365
9. van Dijk, F. S., Nesbitt, I. M., Zwikstra, E. H., Nikkels, P. G., Piersma, S. R., Fratantoni, S. A., Jimenez, C. R., Huizer, M., Morsman, A. C., Cobben, J. M., van Roij, M. H., Elting, M. W., Verbeke, J. I., Wijnaendts, L. C., Shaw, N. J., Högler, W., McKeown, C., Sistermans, E. A., Dalton, A., Meijers-Heijboer, H., and Pals, G. (2009) *Am. J. Hum. Genet.* **85,** 521–527
10. Cabral, W. A., Makareeva, E., Letocha, A. D., Scribanu, N., Fertala, A., Steplewski, A., Keene, D. R., Persikov, A. V., Leikin, S., and Marini, J. C. (2007) *Hum. Mutat.* **28,** 396–405
11. Choi, J. W., Sutor, S. L., Lindquist, L., Evans, G. L., Madden, B. J., Bergen, H. R., 3rd, Hefferan, T. E., Yaszemski, M. J., and Bram, R. J. (2009) *PLoS. Genet.* **5,** e1000750
12. Vranka, J. A., Sakai, L. Y., and Bächinger, H. P. (2004) *J. Biol. Chem.* **279,** 23615–23621
13. Weis, M. A., Hudson, D. M., Kim, L., Scott, M., Wu, J. J., and Eyre, D. R. (2010) *J. Biol. Chem.* **285,** 2580–2590
14. Ishikawa, Y., Wirz, J., Vranka, J. A., Nagata, K., and Bächinger, H. P. (2009) *J. Biol. Chem.* **284,** 17641–17647
15. Sillence, D. O., Ritchie, H. E., and Selby, P. B. (1987) *Am. J. Med. Genet.* **27,** 75–85
16. Shevchenko, A., Tomas, H., Havlis, J., Olsen, J. V., and Mann, M. (2006) *Nat. Protoc.* **1,** 2856–2860
17. Aoyama, C., Santa, T., Tsunoda, M., Fukushima, T., Kitada, C., and Imai, K. (2004) *Biomed. Chromatogr.* **18,** 630–636
18. Corsi, A., Xu, T., Chen, X. D., Boyde, A., Liang, J., Mankani, M., Sommer, B., Iozzo, R. V., Eichstetter, I., Robey, P. G., Bianco, P., and Young, M. F. (2002) *J. Bone Miner. Res.* **17,** 1180–1189
19. Yadav, V. K., and Karsenty, G. (2009) *Aging* **1,** 954–956
20. Yadav, V. K., Oury, F., Suda, N., Liu, Z. W., Gao, X. B., Confavreux, C., Klemenhagen, K. C., Tanaka, K. F., Gingrich, J. A., Guo, X. E., Tecott, L. H., Mann, J. J., Hen, R., Horvath, T. L., and Karsenty, G. (2009) *Cell* **138,** 976–989
21. Fietzek, P. P., Rexrodt, F. W., Hopper, K. E., and Kühn, K. (1973) *Eur. J. Biochem.* **38,** 396–400
22. Rexrodt, F. W., Fietzek, P. P., and Kühn, K. (1975) *Eur. J. Biochem.* **59,** 105–112
23. Fietzek, P. P., Wendt, P., Kell, I., and Kühn, K. (1972) *FEBS Lett.* **26,** 74–76
24. Kefalides, N. A. (1972) *Biochem. Biophys. Res. Commun.* **47,** 1151–1158
25. Rhodes, R. K., and Miller, E. J. (1978) *Biochemistry* **17,** 3442–3448
26. Kefalides, N. A. (1973) *Int. Rev. Connect Tissue Res.* **6,** 63–104
27. Mizuno, K., Peyton, D. H., Hayashi, T., Engel, J., and Bächinger, H. P. (2008) *FEBS J* **275,** 5830–5840